J Nanopart Res (2013) 15:2146
DOI 10.1007/s11051-013-2146-8

RESEARCH PAPER

Dextran-encapsulated barium sulfate nanoparticles prepared for aqueous dispersion as an X-ray contrast agent

Matthew J. Meagher · Bridget Leone · Travis L. Turnbull · Ryan D. Ross · Zhenyuan Zhang · Ryan K. Roeder

Received: 22 September 2013 / Accepted: 18 November 2013 / Published online: 30 November 2013

Abstract Barium sulfate ($BaSO_4$) nanoparticles (<100 nm) are of interest to provide improved performance over microscale $BaSO_4$ particles, which are currently used clinically as an X-ray contrast agent or radiopacifier, and to further enable passive or targeted delivery of $BaSO_4$ contrast agents. The stability of $BaSO_4$ nanoparticle dispersions in aqueous media is critical for these uses but has received little attention. Therefore, the objective of this study was to prepare and characterize a $BaSO_4$ nanoparticle contrast agent with colloidal stability in aqueous media. Monodisperse $BaSO_4$ nanoparticles, ~13 nm in diameter, were synthesized using water-in-oil nanoemulsions wherein the aqueous droplet size limited particle growth and the surfactant layer provided a barrier against aggregation. The as-synthesized nanoparticles were readily redispersed in organic solvents but agglomerated when redispersed in aqueous media due to exhibiting a low, nearly isoelectric zeta potential at neutral pH. Therefore, the as-synthesized $BaSO_4$ nanoparticles were subsequently encapsulated by crosslinked dextran within the nanoemulsion droplets in order to provide both steric and electrostatic stabilization upon breaking the nanoemulsion. Dextran encapsulation increased the particle diameter to ~40 nm, but enabled $BaSO_4$ nanoparticles to be readily redispersed in water and maintain colloidal stability for more than a month. The X-ray attenuation of dispersed dextran-encapsulated $BaSO_4$ nanoparticles was not different from that measured for either a commercial microscale $BaSO_4$ suspension or a solution of barium ions prepared in water at an equal mass concentration of barium, but was significantly greater than the attenuation exhibited by soft tissues. Thus, dextran-encapsulated $BaSO_4$ nanoparticles appear to be suitable for passive or targeted delivery as an X-ray contrast agent.

Keywords Barium sulfate · Dextran · Colloidal stability · Nanoparticles · Nanoemulsion · X-ray contrast agent · Tissue imaging · Nanomedicine

M. J. Meagher · B. Leone · T. L. Turnbull · R. D. Ross · Z. Zhang · R. K. Roeder (✉)
Bioengineering Graduate Program, Department of Aerospace and Mechanical Engineering, University of Notre Dame, 148 Multidisciplinary Research Building, Notre Dame, IN 46556, USA
e-mail: rroeder@nd.edu

Introduction

Barium sulfate ($BaSO_4$) is used clinically as a contrast agent for gastrointestinal radiography (Skucas 1989) and as a radiopacifer in acrylic bone cement (Lewis 1997) due to exhibiting high X-ray attenuation, insolubility, and biocompatibility. Current commercial products for either application use microscale $BaSO_4$ particles; however, $BaSO_4$ nanoparticles could provide improved performance. $BaSO_4$ nanoparticles

improved the mechanical properties of acrylic bone cement compared to microscale particles (Gomoll et al. 2008; Ricker et al. 2008; Gillani et al. 2010). Both $BaSO_4$ (Ricker et al. 2008; Gillani et al. 2010) and gold nanoparticles (Xu et al. 2008) were also reported to exhibit enhanced radiographic contrast compared to microscale particles.

Nanoparticles could also enable intravenous and/or targeted delivery of $BaSO_4$ contrast agents. Nanoparticles can provide enhanced radiographic contrast compared to molecular agents due to delivering a greater mass concentration per particle (Yu and Watson 1999) and offer an ideal platform for designing multi-functional probes for imaging, sensing, and drug delivery (De et al. 2008). Gold nanoparticles have been heavily investigated (Boisseler and Astruc 2009) and have demonstrated utility for vascular imaging (Hainfeld et al. 2006; Cai et al. 2007; Galper et al. 2012) and targeted delivery (Popovtzer et al. 2008; Chanda et al. 2010; Hainfeld et al. 2011; Ross et al. 2012), but options for other lower cost nanoparticle compositions exhibiting high X-ray attenuation are lacking.

$BaSO_4$ exhibits a broad range of high attenuation due to a *K*-absorption edge at $\sim$37 keV, which is at the lower end of the photon energy range utilized by many commercial preclinical and clinical imaging instruments (Berger et al. 2010). For example, a $BaSO_4$ contrast agent recently enabled non-invasive, three-dimensional imaging of microcracks in mineralized tissues using micro-computed tomography (micro-CT) (Landrigan et al. 2010, 2011; Turnbull et al. 2011). However, this technique is currently limited to ex vivo histology, as microscale $BaSO_4$ particles are precipitated within tissue using staining solutions that are not biocompatible. A deliverable $BaSO_4$ contrast agent would require nanoparticles $<$100 nm in diameter for vascular transport, including the lacunar-canalicular network of bone, and extravasation (Knothe-Tate et al. 1998; Gaumet et al. 2008; Albanase et al. 2012).

Realization of the above benefits is dependent on the ability to readily synthesize monodisperse $BaSO_4$ nanoparticles that exhibit colloidal stability in aqueous media. Previous attempts to synthesize submicron $BaSO_4$ particles have included direct precipitation (Uchida et al. 2001; Leng et al. 2004; Bala et al. 2005; Li et al. 2007), possibly using anionic polyelectrolytes and other additives, and water-in-oil micro- or

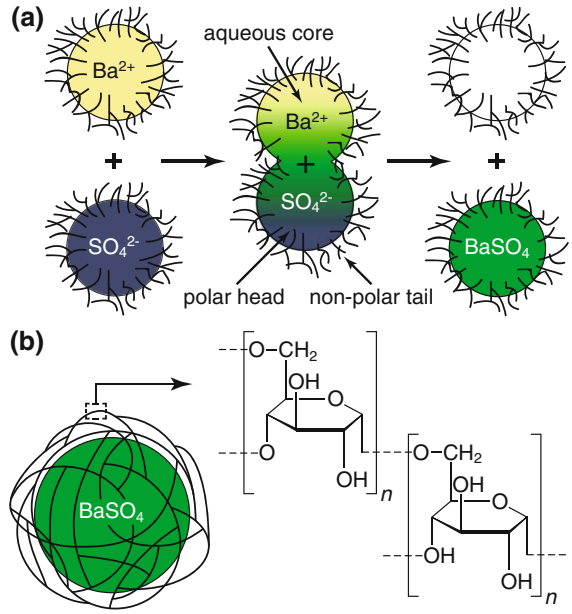

Fig. 1 **a** Schematic diagram showing solute transfer between water-in-oil nanoemulsion droplets. Aqueous droplets suspended via a surfactant in the oil phase controlled primary crystal growth by limiting the available amount of reactants (Ba^{2+} and SO_4^{2-}) and prevented agglomeration by limiting contact between precipitated $BaSO_4$ nanoparticles. **b** Schematic diagram showing encapsulation of $BaSO_4$ nanoparticles within crosslinked dextran, a hydrophilic polysaccharide, to stabilize dispersions in aqueous media

nanoemulsions (Qi et al. 1996; Hopwood and Mann 1997; Ivanova et al. 2001; Koetz et al. 2004; Niemann et al. 2008). Water-in-oil emulsions provide a stable, reliable reaction template for the synthesis of nanoparticles by controlling crystal growth and limiting agglomeration (Fig. 1a) (Qi et al. 1996; Hopwood and Mann 1997; Ivanova et al. 2001; Koetz et al. 2004; Niemann et al. 2008). Aqueous droplets suspended via a surfactant in the oil phase limit (1) primary crystal growth by insuring a large number of nuclei and limiting the available amount of reactants in each aqueous droplet and (2) agglomeration by acting as a physical barrier to contact between the precipitated nanoparticles. The amount of available reactants can be controlled by the salt concentration within aqueous droplets and the droplet size (Qi et al. 1996). The thermodynamic principles governing water-in-oil nanoemulsions facilitate precise control of the droplet size primarily through water/oil/surfactant ratios (Lam et al. 1987; Eastoe and Dalton 2000). However, once the nanoparticles are collected and the stabilizing

effects of the nanoemulsion are removed, the nanoparticles tend to agglomerate into larger aggregates that are not readily redispersed.

The stability of nanoparticle dispersions in aqueous media is critical for clinical use in imaging and drug delivery but thermodynamically challenging due to the high surface energy, thus requiring molecular modifications to provide electrostatic and/or steric stabilization (Wu et al. 2011). For example, the dispersion of superparamagnetic iron oxide nanoparticles, used clinically as a contrast agent for magnetic resonance imaging, has been accomplished by encapsulation within a hydrophilic, biocompatible biopolymer, such as dextran (Palmacci and Josephson 1993; Thorek et al. 2006; Tassa et al. 2011). Encapsulation of $BaSO_4$ nanoparticles within crosslinked dextran (Fig. 1b) would not only confer the hydrophilicity necessary to stabilize the nanoparticles in aqueous media, but could also provide a platform for the covalent attachment of functional groups necessary for targeted delivery (Tassa et al. 2011).

Therefore, the objective of this study was to prepare a $BaSO_4$ nanoparticle contrast agent with colloidal stability in aqueous media. $BaSO_4$ nanoparticles were synthesized using water-in-oil nanoemulsions and stabilized by crosslinked dextran encapsulation. The size distribution of the as-synthesized and dextran-encapsulated $BaSO_4$ nanoparticles was characterized using dynamic light scattering, X-ray diffraction, and electron microscopy. Colloidal stability in aqueous solutions was characterized by zeta potential, and X-ray attenuation was measured by micro-CT.

Experimental methods

$BaSO_4$ nanoparticle synthesis

$BaSO_4$ nanoparticles were prepared by a precipitation reaction,

$$BaCl_2(aq) + (NH_4)_2SO_4(aq) \rightarrow BaSO_4(ppt) + 2\ NH_4Cl(aq) \quad (1)$$

confined by the aqueous droplets within water-in-oil nanoemulsions (Fig. 1a). Reactant solutions were prepared comprising 0.3 M barium chloride, $BaCl_2{\cdot}2H_2O$ (Sigma-Aldrich, ACS Reagent, 99 % purity), and ammonium sulfate, $(NH_4)_2SO_4$ (Sigma-Aldrich, 99.999 % purity), in deionized (DI) water. Nanoemulsions were prepared comprising 90 vol% cyclohexane, C_6H_6 (Sigma-Aldrich, 99.9 % purity), as the oil phase and 10 vol% of a surfactant blend. The surfactant blend was prepared by combining Triton X-100, t-Oct-C_6H_4-$(OCH_2CH_2)_xOH$ (x = 9–10, Sigma-Aldrich, 99.99 % purity), and 1-hexanol, $CH_3(CH_2)_4CH_2OH$ (Sigma-Aldrich, Reagent Grade, 99 % purity), at a weight ratio of 4.5:1. Nanoemulsions for each reactant solution were prepared by adding 1.2 vol% of the aqueous salt solution and mixing until isotropic. $BaCl_2$ and $(NH_4)_2SO_4$ nanoemulsions were added together and stirred vigorously for 90 min to allow equilibration between the aqueous droplets and precipitation of $BaSO_4$ nanoparticles.

Dextran encapsulation

Two additional water-in-oil nanoemulsions were prepared with aqueous droplets containing 8.3 wt% dextran, $(C_6H_{10}O_5)_n$ (n = 9,000–11,000, from *Leuconostoc mesenteroides,* Sigma-Aldrich) (Fig. 1b), and 0.002 M epichlorohydrin, C_3H_5ClO (Sigma, 99 % purity) (Özdemir et al. 2007) in DI water using the same oil phase, surfactant blend, and aqueous phase concentration as described above for the $BaCl_2$ and $(NH_4)_2SO_4$ nanoemulsions. The dextran-containing nanoemulsion was added to the $BaSO_4$-containing nanoemulsion and mixed for 90 min to coat the $BaSO_4$ nanoparticles via droplet exchange. After equilibrating, the epichlorohydrin-containing nanoemulsion was added and mixed for an additional 90 min to crosslink the dextran coating via droplet exchange.

Nanoparticle collection

The nanoemulsion was broken by adding 12.5 vol% acetone and the as-synthesized $BaSO_4$ nanoparticles were collected by centrifugation at 5,000 rpm for 10 min. Following centrifugation, the supernatant was removed from the solution, and the collected particles were washed with ethanol. The centrifugation and washing procedures were repeated three times. Residual ethanol was evaporated at 80–90 °C.

Characterization

The droplet size distribution of each nanoemulsion, and the particle size distribution of the as-synthesized and dextran-encapsulated $BaSO_4$ nanoparticles, was

measured using dynamic light scattering (DLS, Zetasizer Nano-ZS, Malvern Instruments) on 1-mL aliquots in a quartz cuvette. The kinematic viscosity of nanoemulsions was measured using a vibrational viscometer (SV-10, A&D Company, Ltd.) for 10-mL aliquots under ambient conditions.

The crystallographic phase and composition of the as-synthesized nanoparticles were verified by X-ray diffraction (XRD) using Cu Kα radiation generated at 40 kV and 30 mA (X1 Advanced Diffraction System, Scintag, Inc.). Nanoparticles were examined over 15–80° two-theta with a step size of 0.02° and a step time of 0.04 s. The primary crystallite size was measured from peak broadening in XRD using the Scherrer equation (Cullity 1978). The full-width-at-half-maximum peak breadths were measured for the 111, 021, 210, 121, 211, 002, 122, 140, and 212 reflections after profile fitting using a Pearson VII function. Instrument broadening was corrected using Warren's method with a microscale control sample (Cullity 1978). Hall-Williamson analysis (Williamson and Hall 1953) revealed that the effect of lattice strain was not statistically significant by least squares linear regression ($p = 0.56$); therefore, the crystallite size was determined as the mean (±standard deviation) of measurements for each individual reflection.

The morphology and particle size distribution of the as-synthesized and dextran-encapsulated $BaSO_4$ nanoparticles were also characterized by transmission electron microscopy (TEM, Hitachi H-600) and scanning electron microscopy (SEM, Evo 50, LEO Electron Microscopy Ltd.), respectively. TEM specimens were prepared by immersing carbon-coated grids in nanoparticle dispersions and evaporating the solvent. SEM specimens were prepared by placing drops of nanoparticle dispersions onto SEM sample holders, evaporating the solvent, and coating with Au by sputter deposition. The mean (±standard deviation) particle diameter was measured from a sample of 50 particles in micrographs using common stereological methods (ImageJ).

The electrokinetic or zeta potential (ζ-potential) of the as-synthesized and dextran-encapsulated $BaSO_4$ nanoparticles was measured via electrophoretic mobility (Zetasizer Nano-ZS, Malvern Instruments) under ambient conditions as a function of pH (Hang et al. 2007). Nanoparticle dispersions containing 2.5 mg/mL $BaSO_4$ in DI water were titrated (MPT-2 Autotitrator, Malvern Instruments) from neutral pH to acidic and basic conditions using 0.01, 0.1 or 1.0 M solutions of HCl and NaOH, respectively. All measurements were performed in triplicate and reported as the mean (±standard deviation).

The X-ray attenuation of dextran-encapsulated $BaSO_4$ nanoparticles was measured using micro-CT and compared to a commercial microscale $BaSO_4$ suspension and a solution of dissolved Ba^{2+} ions, each prepared at an equal mass concentration of Ba. Dextran-encapsulated $BaSO_4$ nanoparticles were dispersed in DI water and placed in 10-mm diameter sample tubes at a concentration of 0.01 g/mL. The commercial microscale $BaSO_4$ suspension (E-Z-HD^{TM}, 98 % w/w $BaSO_4$ suspension, E-Z-EM Inc.) was diluted in DI water to 0.01 g/mL and also placed in sample tubes; the mean (±standard deviation) particle diameter was 834 (±370) nm as measured from a sample of 50 particles in SEM micrographs using common stereological methods (ImageJ). A solution of Ba^{2+} ions was prepared by dissolving 0.04 M $BaCl_2{\cdot}2H_2O$ in DI water. Settling of the microscale $BaSO_4$ suspension during imaging was prevented by dissolving 0.4 g/mL polyvinyl alcohol (PVA), $(CH_2CHOH)_n$ (P1763, Sigma-Aldrich), in microscale suspensions, nanoparticle dispersions, and Ba^{2+} ion solutions to form hydrogels within the sample tubes. Each sample ($n = 3$–5/group) was imaged by micro-CT (μCT-80, Scanco Medical AG, Brüttisellen, Switzerland) at 70 kVp, 114 mA, and 400-ms integration time for 10 slices with a 10-μm voxel size and 0.5-mm Al filter. The measured linear attenuation coefficient was converted to Hounsfield units (HU) using an internal linear calibration against air (−1000 HU) and water (0 HU) for each sample. Groups were compared using Kruskal–Wallis nonparametric analysis of variance (ANOVA) with a level of significance set at 0.05 (JMP 10, SAS Institute).

Results and discussion

Nanoemulsion characterization

The isotropic phase of the water-in-oil nanoemulsion was qualitatively characterized by optical clarity and decreased kinematic viscosity. Kinematic viscosity measurements above 3 mPa s indicated a non-isotropic nanoemulsion, while kinematic viscosity measurements ≤2.7 mPa s indicated an isotropic

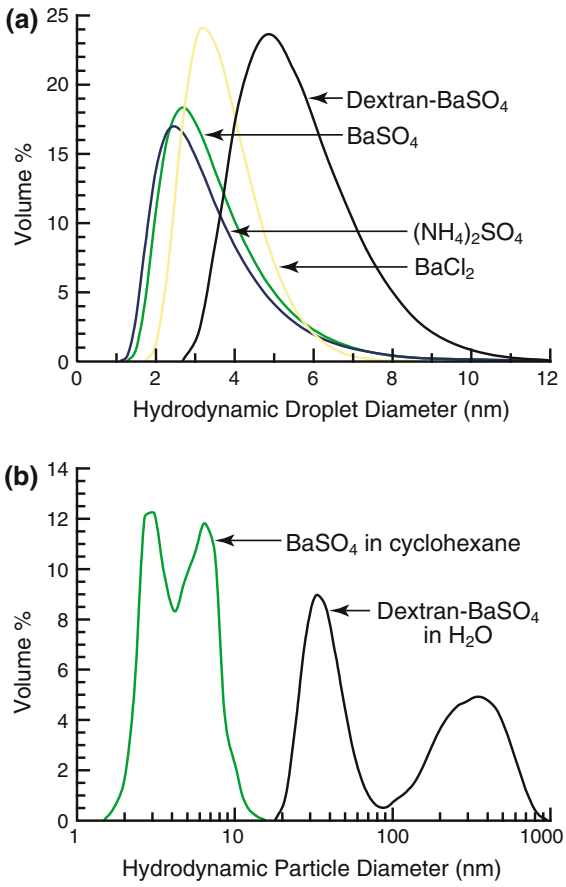

Fig. 2 **a** Droplet size distributions measured by DLS for nanoemulsions containing Ba^{2+}, SO_4^{2-}, precipitated $BaSO_4$ nanoparticles and dextran-encapsulated $BaSO_4$ nanoparticles. **b** Particle size distributions measured by DLS for the as-synthesized $BaSO_4$ nanoparticles redispersed in cyclohexane and dextran-encapsulated $BaSO_4$ nanoparticles redispersed in water

nanoemulsion. Once equilibrated, an isotropic nanoemulsion remained stable for at least 7 days, as evidenced by the stability of droplet size distributions measured via DLS. Nanoemulsions containing $BaCl_2$ and $(NH_4)_2SO_4$ reactants, as well as precipitated $BaSO_4$ nanoparticles, exhibited a narrow droplet size distribution with a mean hydrodynamic diameter of $\sim$3 nm (Fig. 2a). Nanoemulsions containing dextran-encapsulated $BaSO_4$ nanoparticles also exhibited a monodispersed droplet size distribution, but a slightly larger mean hydrodynamic diameter ($\sim$5 nm) compared to the constituent nanoemulsions (Fig. 2a).

A theoretical yield of 4.8×10^{-4} mol (0.112 g) of $BaSO_4$ was expected for nanoemulsions containing 0.3 M salt solutions. Following reaction, $\sim 4.2 \times 10^{-4}$ mol (0.100 g) of $BaSO_4$ was typically collected for a yield of 89 %. Losses from the theoretical yield were attributed to incomplete exchange of Ba^{2+} and SO_4^{2-} salts between nanoemulsion droplets, and not incomplete collection of precipitated nanoparticles, due to the ability to precipitate $BaSO_4$ from the supernatant solution after the collection of nanoparticles.

Nanoemulsions enabled the synthesis of monodispersed $BaSO_4$ nanoparticles by controlling crystal nucleation, growth, and agglomeration. Aqueous droplets in the water-in-oil nanoemulsion served as "nanoreactors" or templates by confining the aqueous reactants and crystalline product within an elastic surfactant film (Fig. 1a). Monodisperse, nanoscale droplets, <10 nm in diameter, were facilitated using a water content which was lower than previous studies (Qi et al. 1996; Hopwood and Mann 1997). The small droplet size subsequently produced a small crystal size by providing a large number nucleation sites and limiting the amount of reactants available for precipitation and crystal growth. Moreover, the surfactant film provided an elastic, steric barrier to limit particle growth and aggregation. However, the mean droplet diameter after precipitation of $BaSO_4$ nanoparticles was smaller than the mean diameter of collected $BaSO_4$ nanoparticles (Fig. 2b, 3a). This suggests that either (1) the elastic surfactant film confining aqueous droplets was able to stretch to accommodate some crystal growth, or (2) droplets or particles underwent slight aggregation during mixing or breaking the nanoemulsion, respectively. In either case, the overall droplet size distribution was unaffected by the precipitation of $BaSO_4$ nanoparticles (Fig. 2a) due to (1) containing a relatively small number of droplets containing precipitated $BaSO_4$ nanoparticles or (2) preceding any particle aggregation.

Nanoparticle characterization

The as-synthesized $BaSO_4$ nanoparticles readily agglomerated when redispersed in polar solvents such as water after collection from the nanoemulsion. Therefore, the as-synthesized $BaSO_4$ nanoparticles were initially redispersed in cyclohexane for characterization via DLS and TEM. The mean hydrodynamic diameter measured by DLS was $\sim$5 nm, and the entire size distribution was <15 nm (Fig. 2b).

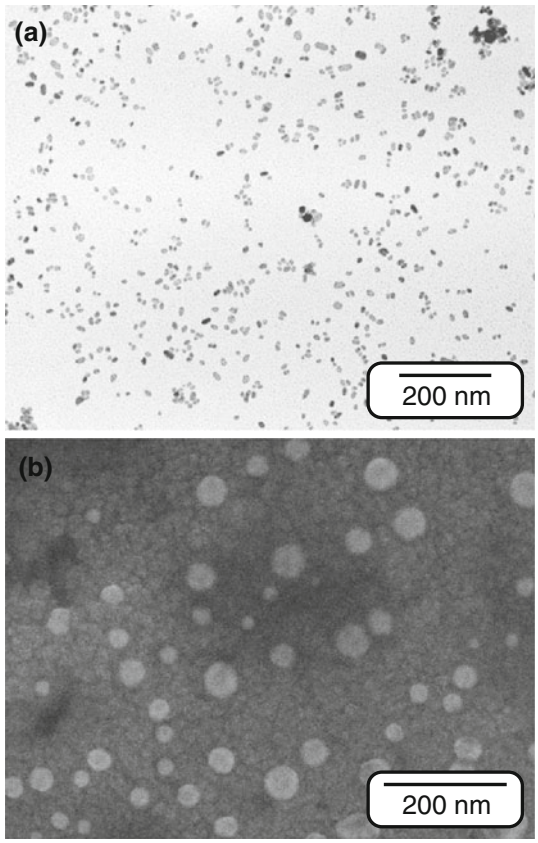

Fig. 3 **a** Representative TEM micrograph showing the as-synthesized $BaSO_4$ nanoparticles collected from dispersion in cyclohexane and **b** representative SEM micrograph showing the as-synthesized, dextran-encapsulated $BaSO_4$ nanoparticles collected from dispersion in water

The as-synthesized $BaSO_4$ nanoparticles redispersed in cyclohexane were directly observed in TEM to exhibit monodispersed ellipsoidal nanoparticles with a mean diameter of 12.5 (±4.7) nm (Fig. 3a). The crystallographic phase of the as-synthesized nanoparticles was verified to be $BaSO_4$ by XRD (Fig. 4). A primary crystallite diameter of 15.3 (±3.4) nm was measured from peak broadening. Thus, particle size measurements from DLS, TEM, and XRD were in reasonable agreement.

Nanoparticle dispersion

The as-synthesized $BaSO_4$ nanoparticles remained dispersed and stable while contained within the aqueous nanoemulsion droplets surrounded by a surfactant film, but readily formed agglomerates at least 250 nm in diameter when the stabilizing effects

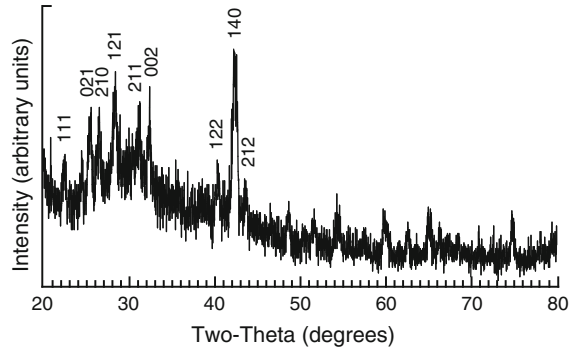

Fig. 4 Powder XRD pattern for the as-synthesized $BaSO_4$ nanoparticles. All peaks corresponded to $BaSO_4$ (JCPDS 1997). Reflections used for crystallite size measurement are indexed

of the nanoemulsion were removed. The collected, agglomerated nanoparticles were readily redispersed in organic solvents such as cyclohexane, as described above (Fig. 2b, 3a). However, aqueous dispersion was inhibited by a low zeta potential measured to be +1.6 (±1.1) mV at neutral pH (Fig. 5). This low, nearly isoelectric zeta potential was consistent with a previous study which measured an isoelectric point at pH ~7–8 for ~40 nm $BaSO_4$ nanoparticles in the absence of counterions and at a similar solids loading (Hang et al. 2007). The zeta potential required for purely electrostatic stabilization of colloidal particles is typically taken as ±25–30 mV (Riddick 1968; Balastre et al. 2002). Colloidal stability at lower zeta potential thus requires steric stabilization.

Dextran encapsulation of $BaSO_4$ nanoparticles provided colloidal stability in aqueous media. The size distribution measured by DLS was bimodal with peaks spanning 20–80 and 100–800 nm, but the mean hydrodynamic diameter of the primary peak was ~37 nm (Fig. 2b). The larger peak was most likely due to excess dextran and was readily separated from the nanoparticles. The dextran-encapsulated $BaSO_4$ nanoparticles were readily redispersed in water and were directly observed in SEM to be spherical with a mean diameter of 39.6 (±11.7) nm (Fig. 3b), which was consistent with the primary peak of the bimodal size distribution measured by DLS. Thus, dextran encapsulation resulted in a three- to four-fold increase in particle size, due to a dextran coating ~10–15 nm in thickness, which provided a hydrophilic coating and steric barrier to agglomeration.

Dextran-encapsulated $BaSO_4$ nanoparticles were readily redispersed in water and remained stable. After

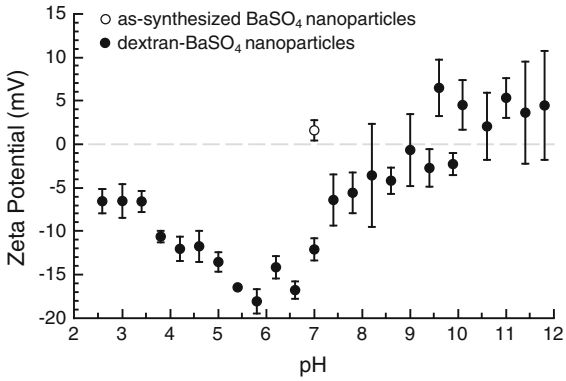

Fig. 5 Zeta potential of the as-synthesized and dextran-encapsulated $BaSO_4$ nanoparticles measured as a function of pH at 2.5 mg/mL $BaSO_4$ in DI water. *Error bars* show one standard deviation of the mean. At neutral pH, the as-synthesized nanoparticles readily agglomerated, but dextran-encapsulated nanoparticles were stable, despite exhibiting a relatively low zeta potential, due to steric stabilization from the crosslinked dextran coating

1 month, dextran-encapsulated $BaSO_4$ nanoparticles remained well-dispersed, but the hydrodynamic diameter was increased to $\sim$60 nm, most likely due to swelling or degradation of the dextran coating. The zeta potential of dextran-encapsulated $BaSO_4$ nanoparticles as-prepared was measured to be -12.1 (± 1.3) mV at neutral pH, and was negative over a wide range of pH (Fig. 5). The zeta potential reached a maxima near neutral pH and decreased in magnitude under alkaline conditions. The behavior under alkaline conditions was unexpected and possibly due to degradation of the dextran coating, which was previously observed in crosslinked dextran hydrogels (Kim et al. 1999). The negative zeta potential measured at neutral pH suggested that the hydrophilic crosslinked dextran coating provided both electrostatic and steric stabilization.

To the authors' knowledge, this study marks the first use of dextran encapsulation to stabilize $BaSO_4$ nanoparticles in aqueous media. Crosslinked dextran coatings were previously used to provide hydrophilicity and aqueous stability to superparamagnetic iron oxide nanoparticles, which are now commercially available for clinical use as a contrast agent for magnetic resonance imaging (Palmacci and Josephson 1993; Thorek et al. 2006; Tassa et al. 2011). Therefore, the dextran coating and low surface charge are expected to promote biocompatibility, stability in physiologic media containing buffers and proteins (Palmacci and Josephson 1993; Thorek et al. 2006; Tassa et al. 2011), and a relativity long circulation half-life in vivo (Albanse et al. 2012), but further experiments are required for verification. Furthermore, active targeting can be facilitated via covalent attachment of functional ligands to dextran (Tassa et al. 2011).

A possible limitation of dextran encapsulation is the inherent increase in particle size. The increase in nanoparticle size from $<$10 to $\sim$40 nm due to the dextran coating thickness may limit delivery and the biodistribution, but may also increase the circulation half-life (Albanase et al. 2012). The increased particle size and negative zeta potential under acidic conditions suggest that nanoparticles in this study were encapsulated with an excess of dextran. Thus, the dextran coating thickness could be tailored via the dextran molecular weight and/or concentration in nanoemulsion droplets.

X-ray attenuation

Dextran-encapsulated $BaSO_4$ nanoparticles exhibited no difference in X-ray attenuation compared to either a commercial microscale $BaSO_4$ suspension or a solution of dissolved Ba^{2+} ions ($p = 0.35$, ANOVA), each prepared at an equal mass concentration of Ba and using a PVA dispersant to maintain stability of the microscale suspension (Fig. 6). The measured X-ray attenuation was $\sim$150 HU, which was significantly greater than the attenuation of soft tissues (Fig. 6) even at a relatively low Ba concentration (0.01 g/ml). For comparison, the recommended concentration of the commercial microscale $BaSO_4$ suspension is $\sim$5 g/ml for clinical gastrointestinal imaging (E-Z-HD^{TM}, E-Z-EM Inc.).

The results of this study also raise questions regarding other recent studies which reported enhanced radiographic contrast for $BaSO_4$ and gold nanoparticles compared to microscale particles (Ricker et al. 2008; Gillani et al. 2010; Xu et al. 2008). The reported effects of particle size on radiographic contrast in these studies could not have been due to the physical effects of particle size, but were likely due to concomitant differences in dispersion and thus mass concentration. At the photon energy levels used in radiography and computed tomography, the X-ray attenuation of high atomic number elements is governed by photoelectric absorption due to differences in

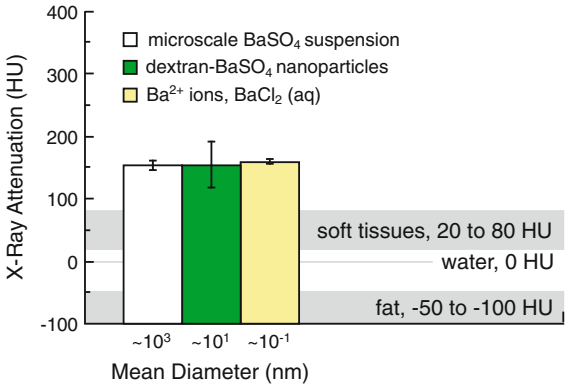

Fig. 6 The X-ray attenuation of a commercial microscale $BaSO_4$ suspension, dextran-encapsulated $BaSO_4$ nanoparticles, and a solution of dissolved Ba^{2+} ions ($BaCl_2$) was not statistically different ($p = 0.35$, ANOVA) but was significantly greater than that exhibited by soft tissues. Samples from each group were prepared at an equal mass concentration of Ba (0.01 g/mL) and an equal concentration of PVA (0.4 g/mL) added to insure stability of the microscale suspension. *Error bars* show one standard deviation of the mean

mass concentration, while scattering processes, which could be partially influenced by differences in specific surface area, are insignificant in comparison (Hubbell 1969; Hubbell et al. 1980; Hubbell and Seltzer 2004; Berger et al. 2010). Therefore, the results of this study confirmed no measurable effect of nanoparticle size on X-ray attenuation in X-ray absorption imaging systems. Moreover, the range of scale investigated in this study spanned four orders of magnitude from Ba^{2+} ions to microscale particles (Fig. 6). Similar results were also simultaneously confirmed in our laboratory for gold nanoparticles (Ross et al. 2013).

Therefore, a decreased particle size has no benefit for X-ray contrast at equal mass concentration, but this does not preclude other potential benefits. Decreased particle size in $BaSO_4$ suspensions has been implicated with improved stability, which can enable more uniform coating and thus improved radiographic imaging of the gastrointestinal tract (Gelfand and Ott 1982). Moreover, surface functionalization of dextran-encapsulated $BaSO_4$ nanoparticles could provide a platform to investigate targeted labeling of polyps in gastrointestinal imaging, which could improve specificity (O'Connor and Summers 2007) and decrease the administered dose of $BaSO_4$. Finally, $BaSO_4$ nanoparticles could also provide a lower cost alternative to gold nanoparticles for passive or targeted delivery as an X-ray contrast agent.

Conclusions

Monodisperse $BaSO_4$ nanoparticles, $\sim$13 nm in diameter, were synthesized using water-in-oil nanoemulsions wherein the aqueous droplet size limited particle growth and the surfactant layer provided a barrier against aggregation. The as-synthesized nanoparticles were readily redispersed in organic solvents but agglomerated when redispersed in aqueous media due to exhibiting a low, nearly isoelectric zeta potential at neutral pH. Therefore, the as-synthesized $BaSO_4$ nanoparticles were subsequently encapsulated by crosslinked dextran within the nanoemulsion droplets in order to provide both steric and electrostatic stabilization upon breaking the nanoemulsion. Dextran encapsulation increased the particle diameter to $\sim$40 nm, but enabled $BaSO_4$ nanoparticles to be readily redispersed in water and remain stable for more than 1 month. The X-ray attenuation of dextran-encapsulated $BaSO_4$ nanoparticles was not different from that measured for either a commercial microscale $BaSO_4$ suspension or a solution of barium ions prepared at an equal mass concentration of barium, but was significantly greater than the attenuation exhibited by soft tissues. Thus, dextran-encapsulated $BaSO_4$ nanoparticles appear to be suitable for passive or targeted delivery as an X-ray contrast agent.

Acknowledgments This research was supported by the U.S. Army Medical Research and Materiel Command (W81XWH-06-1-0196) through the Peer Reviewed Medical Research Program (PR054672). The authors acknowledge the Notre Dame Integrated Imaging Facility (NDIIF) for the use of TEM and SEM.

References

Albanase A, Tang PS, Chan WCW (2012) The effect of nanoparticle size, shape, and surface chemistry on biological systems. Annu Rev Biomed Eng 14:1–16

Bala H, Fu W, Zhao J, Ding X, Jiang Y, Yu K, Wang Z (2005) Preparation of $BaSO_4$ nanoparticles with self-dispersing properties. Colloids Surf A 252:129–134

Balastre M, Argillier JF, Allain C, Foissy A (2002) Role of polyelectrolyte dispersant in the settling behaviour of barium sulphate suspension. Colloids Surf A 211:145–156

Berger MJ, Hubbell JH, Seltzer SM, Chang J, Coursey JS, Sukumar R, Zucker DS, Olsen K (2010) XCOM: Photon Cross Section Database. National Institute of Standards and Technology: Gaithersburg, MD. http://physics.nist.gov/xcom. Accessed 22 Sep 2013

Boisselier E, Astruc D (2009) Gold nanoparticles in nanomedicine: preparations, imaging, diagnostics, therapies and toxicity. Chem Soc Rev 38:1759–1782

Cai QY, Kim SH, Choi KS, Kim SY, Byun SJ, Kim KW, Park SH, Juhng SK, Yoon K-H (2007) Colloidal gold nanoparticles as a blood-pool contrast agent for X-ray computed tomography in mice. Invest Radiol 42(12):797–806

Chanda N, Kattumuri V, Shukla R, Zambre A, Katti K, Upendran A, Kulkami RR, Kan P, Fent GM, Casteel SW, Smith CJ, Boote E, Robertson JD, Cutler C, Lever JR, Katti KV, Kannan R (2010) Bombesin functionalized gold nanoparticles show in vitro and in vivo cancer receptor specificity. Proc Natl Acad Sci 107(10):8760–8765

Cullity B (1978) Elements of X-ray diffraction. Addison-Wesley Publishing Company Inc, Reading, MA, pp 281–285

De M, Ghosh PS, Rotello VM (2008) Applications of nanoparticles in biology. Adv Mater 20(22):4225–4241

Eastoe J, Dalton JS (2000) Dynamic surface tension and adsorption mechanisms of surfactants at the air-water interface. Adv Colloid Interface Sci 85:103–144

Galper MW, Saung MT, Fuster V, Roessl E, Thran A, Proksa R, Fayad ZA, Cormode DP (2012) Effect of computed tomography scanning parameters on gold nanoparticle and iodine contrast. Invest Radiol 47(8):475–481

Gaumet M, Vargas A, Gurny R, Delie F (2008) Nanoparticles for drug delivery: the need for precision in reporting particle size parameters. Eur J Pharm Biopharm 69:1–9

Gelfand DW, Ott DJ (1982) Barium sulfate suspensions: an evaluation of available products. Am J Roentgenol 138(5):935–941

Gillani R, Ercan B, Qiao A, Webster TJ (2010) Nanofunctionalized zirconia and barium sulfate particles as bone cement additives. Int J Nanomed 5(1):1–11

Gomoll AH, Fitz W, Scott RD, Thornhill TS, Bellare A (2008) Nanoparticulate fillers improve the mechanical strength of bone cement. Acta Orthop 79:421–427

Hainfeld JF, Slatkin DN, Focella TM, Smilowitz HM (2006) Gold nanoparticles: a new X-ray contrast agent. Brit J Radiol 79(939):248–253

Hainfeld JF, O'Connor MJ, Bilmanian FA, Slatkin DN, Adams DJ, Smilowitz HM (2011) Micro-CT enables microlocalisation and quantification of Her2-targeted gold nanoparticles within tumour regions. Brit J Radiol 84(1002):526–533

Hang JZ, Zhang YF, Shi LY, Feng X (2007) Electrokinetic properties of barite nanoparticles suspensions in different electrolyte media. J Mater Sci 42:9611–9616

Hopwood JD, Mann S (1997) Synthesis of barium sulfate nanoparticles and nanofilaments in reverse micelles and microemulsions. Chem Mater 9:1819–1828

Hubbell JH (1969) Photon cross sections, attenuation coefficients, and energy absorption coefficients from 10 keV to 100 GeV. Nat Stand Ref Data Ser 29:85

Hubbell JH, Seltzer SM (2004) Table of X-ray Mass Attenuation Coefficients and Mass Energy-Absorption Coefficients (version 1.4). National Institute of Standards and Technology, Gaithersburg, MD. Available at: http://physics.nist.gov/xaamdi. Accessed 22 Sep 2013

Hubbell JH, Gimm HA, Overbo I (1980) Pair, triplet, and total atomic cross sections (and mass attenuation coefficients) for 1 MeV–100 GeV photons in elements $Z = 1$ to 100. J Phys Chem Ref Data 9:1023–1147

Ivanova NI, Rudelev DS, Summ BD, Chalykh AA (2001) Synthesis of barium sulfate nanoparticles in water-in-oil microemulsion systems. Colloid J 63(6):714–717

JCPDS (1997), Powder Diffraction File 24-1035, $BaSO_4$, Barium Sulfate. JCPDS—International Center for Diffraction Data (ICDD), Newton Square, PA

Kim S-H, Won C-Y, Chu C-C (1999) Synthesis and characterization of dextran-maleic acid based hydrogel. J Biomed Mater Res 46:160–170

Knothe-Tate ML, Niederer P, Knothe U (1998) In vivo tracer transport though the lacunocanalicular system of rat bone in an environment devoid of mechanical loading. Bone 22(2):107–117

Koetz J, Bahnemann J, Lucas G, Tiersch B, Kosmella S (2004) Polyelectrolyte-modified microemulsions as new templates for the formation of nanoparticles. Colloids Surf A 250:423–430

Lam AC, Falk NA, Schechter RS (1987) The thermodynamics of microemulsions. J Colloid Interface Sci 120:30–41

Landrigan MD, Flatley JC, Turnbull TL, Kruzic JJ, Ferracane JL, Hilton TJ, Roeder RK (2010) Detection of dentinal cracks using contrast enhanced micro-computed tomography. J Mech Behav Biomed Mater 3(2):223–227

Landrigan MD, Li J, Turnbull TL, Burr DB, Niebur GL, Roeder RK (2011) Contrast-enhanced micro-computed tomography of fatigue microdamage accumulation in human cortical bone. Bone 48(3):443–450

Leng H, Wang X, Niebur GL, Roeder RK (2004) Synthesis of a barium sulfate nanoparticle contrast agent for micro-computed tomography of bone microstructure. Ceram Trans 159:219–229

Lewis G (1997) Properties of acrylic bone cement: state of the art review. J Biomed Mater Res (Appl Biomater) 38B:155–182

Li S, Xu J, Luo G (2007) Control of crystal morphology through supersaturation ratio and mixing conditions. J Crystal Growth 304:219–224

Niemann B, Veit P, Sundmacher K (2008) Nanoparticle precipitation in reverse microemulsions: particle formation dynamics and tailoring of particle size distributions. Langmuir 24:4320–4328

O'Connor SD, Summers RM (2007) Revisiting oral barium sulfate contrast agents. Acad Radiol 14:72–80

Özdemir C, Çolak N, Güner A (2007) Solution dynamics of the dextran/crosslinking agent systems. J Appl Polym Sci 105:1177–1187

Palmacci S, Josephson L (1993) Synthesis of polysaccharide covered superparamagnetic oxide colloids. U.S. Patent No. 5 262 176

Popovtzer R, Agrawal A, Kotov NA, Popovtzer A, Balter J, Carey TE, Kopelman R (2008) Targeted gold nanoparticle enable molecular CT imaging of cancer. Nano Lett 8(12):4593–4596

Qi L, Ma J, Cheng H, Zhao Z (1996) Preparation of $BaSO_4$ nanoparticles in non-ionic w/o microemulsions. Colloids Surf A 108:117–126

Ricker A, Liu-Snyder P, Webster TJ (2008) The influence of nano MgO and $BaSO_4$ particle size additives on properties of PMMA bone cement. Int J Nanomed 3(1):125–132

Riddick TM (1968) Control of Colloid Stability Through Zeta Potential. Zeta Meter Inc., New York, NY

Ross RD, Cole LE, Roeder RK (2012) Relative binding affinity of carboxylate-, phosphonate-, and bisphosphonate-functionalized gold nanoparticles targeted to damaged bone tissue. J Nanopart Res 14(10):1175 (6 pages)

Ross RD, Cole LE. Tilley JMR, Roeder RK (2013) Effects of functionalized gold nanoparticle size on X-ray attenuation and binding affinity to hydroxyapatite. Chem Mater, in review

Skucas J (1989) Radiographic contrast agents. Aspen Publishers Inc., Rockville, MD, pp 10–76

Tassa C, Shaw ST, Weissleder R (2011) Dextran-coated iron oxide nanoparticles: a versatile platform for targeted molecular imaging, molecular diagnostics and therapy. Acc Chem Res 44:842–852

Thorek DLJ, Chen AK, Czupryna J, Tsourkas A (2006) Superparamagnetic iron oxide nanoparticle probes for molecular imaging. Ann Biomed Eng 34:23–28

Turnbull TL, Gargac JA, Niebur GL, Roeder RK (2011) Detection of fatigue microdamage in whole rat femora using contrast-enhanced micro-computed tomography. J Biomech 44:2395–2400

Uchida M, Sue A, Yoshioka T, Okuwaki A (2001) Morphology of barium sulfate synthesized with barium(ii)-aminocarboxylate precursors. CrystEngComm 5:1–6

Williamson GK, Hall WH (1953) X-ray line broadening from filed aluminium and wolfram. Acta Metall 1:22–31

Wu L, Zhang J, Watanabe W (2011) Physical and chemical stability of drug nanoparticles. Adv Drug Delivery Rev 63:456–469

Xu C, Tung GA, Sun S (2008) Size and concentration effect of gold nanoparticles on X-ray attenuation as measured on computed tomography. Chem Mater 20(13):4167–4169

Yu S-B, Watson AD (1999) Metal-based X-ray contrast media. Chem Rev 99:2353–2377